Single-species dinoflagellate cyst carbon isotope fractionation in from coretop sediments: environmental controls, CO2-dependency and proxy potential

5   Joost Frieling[1‡], Linda van Roij[1], Iris Kleij[1], Gert-Jan Reichart[1,2] & Appy Sluijs[1]

1. Department of Earth Sciences, Faculty of Geosciences, Utrecht University, Princetonlaan 8, 3584CB Utrecht, The Netherlands

2. NIOZ Royal Netherlands Institute for Sea Research and Utrecht University, Texel, The Netherlands

‡ now at: Department of Earth Sciences, University of Oxford, South Parks Road, Oxford, OX1 3AN, Oxford, United Kingdom

10   *Correspondence to*: A. Sluijs (a.sluijs@uu.nl), J. Frieling (joost.frieling@earth.ox.ac.uk)

Abstract. Sedimentary bulk organic matter and various molecular organic components exhibit strong CO_2-dependent carbon isotope fractionation relative to dissolved inorganic carbon sources. This fractionation (ε_p) has been employed as proxy for paleo-pCO_2. Yet, culture experiments indicate this CO_2-dependent ε_p is highly specific at genus and even species level, potentially hampering the use of bulk organic matter and non-species specific organic compounds. In recent years, significant

15   progress has been made towards a CO_2 proxy using controlled growth experiments with dinoflagellate species, also showing highly species-specific ε_p values. These values were, however, based on motile specimens and it remains unknown whether these relations also hold for the organic-walled resting cysts (dinocysts) produced by these dinoflagellate species in their natural environment. We here analyze dinocysts isolated from core-tops from the Atlantic Ocean and Mediterranean Sea, representing several species (*Spiniferites elongatus, S. (cf.) ramosus, S. mirabilis, Operculodinium centrocarpum* sensu Wall

20   & Dale (1966) (hereafter referred to as *O. centrocarpum*) and *Impagidinium aculeatum*) using Laser ablation – nano Combustion – Gas Chromatography – Isotope Ratio Mass Spectrometry (LA/nC/GC-IRMS). We find that the dinocysts produced in the natural environment are all significantly more ^{13}C-depleted compared to the cultured motile dinoflagellate cells, implying higher overall ε_p values and, moreover, exhibit large isotope variability. Where several species could be analysed from a single location, we often record significant differences in isotopic variance and offsets in mean $\delta^{13}C$ values

25   between species, highlighting the importance of single-species carbon isotope analyses. The most geographically expanded dataset, based on *O. centrocarpum*, shows that ε_p correlates significantly with various environmental parameters. Importantly, *O. centrocarpum* shows a CO_2-dependent ε_p above ~240 µatm pCO_2. Similar to other marine autotrophs, relative insensitivity at low pCO_2 is in line with a carbon concentrating mechanism being active at low pCO_2, although we here cannot fully exclude that we partly underestimated ε_p sensitivity at low pCO_2 values due to the relatively sparse sampling in that range. Finally, we

30   use the relation between ε_p and pCO_2 in *O. centrocarpum* to propose a first pCO_2 proxy based on a single dinocyst species.

1 Introduction

Stable carbon isotope fractionation in marine autotrophs is governed for a large part by the carbon fixing enzyme RubisCO (e.g. Farquhar et al., 1989; Roeske and O'Leary, 1984), which implies most marine organic matter and therefore sedimentary marine organic matter is strongly ^{13}C-depleted with respect to the dissolved inorganic carbon (DIC) source (CO_2 (aq), HCO_3^-

35   or CO_3^{2-}), with the stable carbon isotope composition ($\delta^{13}C$) of organic matter ranging from -10 to -30‰ (Freeman and Hayes, 1992). While many groups of marine autotrophs show clear CO_2-dependent carbon isotope fractionation (ε_p), the exact relation strongly varies between marine phytoplankton groups, genera and cell morphologies (Popp et al., 1998; Boller et al., 2011, 2015). Still, because of the assumed CO_2-dependency of RubisCO fractionation, bulk marine organic matter and more specific organic compounds of marine autotrophs (e.g. lipids biomarkers) have been proposed and applied as pCO$_2$ proxies over the

40   past decades (Freeman and Hayes, 1992; Naafs et al., 2016). The application of these pCO$_2$ proxies (Bijl et al., 2010; Pagani et al., 2011; Schoon et al., 2011; Witkowski et al., 2018) has provided constraints on past atmospheric pCO$_2$ and earth system sensitivity beyond the ice core record (Pagani et al., 2010; PALAEOSENS, 2012).

However, many of the organic compounds used for CO₂ reconstructions are not related to a single species, genus or even group. This implies that reconstructions based on these compounds integrates interspecific differences in CO₂-dependency,

45   which complicates the interpretation of such proxy records. Secondly, even if specific compounds derive from a single species or genus, they intrinsically derive from a multitude of organisms, differing in shape and size, affecting isotopic fractionation and hence limiting the accuracy of such CO₂ reconstructions.

Part of the uncertainties and biases in carbon isotope fractionation can be circumvented if the carbon isotopic fractionation of individual fossils can be analyzed. In recent years, significant progress has been made towards a CO₂ proxy based on the stable

50   carbon isotope fractionation in organic walled dinoflagellate cysts (Burkhardt et al., 1999; Hoins et al., 2015, 2016a, 2016b; Wilkes et al., 2017). A fraction (~15%) of modern dinoflagellates produces an organic resting cyst or dinocyst as an obligatory part of their lifecycle (Evitt, 1985). The organic resting cysts from autotrophic species have excellent preservation potential, are often highly oxidation-resistant (Zonneveld et al., 1997, 2019; Kodrans-Nsiah et al., 2008) and several ubiquitous extant species are extremely long-ranging (Fensome et al., 1996; Williams et al., 2004). The ecology and morphology of these long-

55   ranging species are seemingly unchanged for millions of years (Frieling and Sluijs, 2018). Most importantly, recent advances in methodology allow for analyses of species-specific single-cyst $\delta^{13}C$ (van Roij et al., 2016; Sluijs et al., 2018). This presents the opportunity to quantify environmental controls on ε_p of individual dinoflagellate cysts and hence species to assess the potential to obtain more accurate paleo-pCO$_2$ estimates from sedimentary records.

Controlled growth experiments across a range of CO₂ levels representative for the last glacial (e.g. Barnola et al., 1987),

60   modern and future carbon emission scenarios (Eberlein et al., 2016; Hoins et al., 2016a, 2016b, 2015; IPCC, 2014; Rost et al., 2006; Van de Waal et al., 2013; Wilkes et al., 2017) showed species specific CO₂ dependent ε_p for multiple dinoflagellate species. From these, the species *Protoceratium reticulatum* and *Gonyaulax spinifera* (Hoins et al., 2015, 2016a, 2016b) are of particular interest as these produce the organic cyst species *Operculodinium centrocarpum* sensu Wall and Dale, (1966),

hereafter referred to as *O. centrocarpum,* and *Spiniferites (cf.) ramosus,* hereafter referred to as *S. ramosus*, respectively (Head,
65 1996; Zonneveld et al., 2013). These cyst species have their first occurrences in the geological records around ~60 and 130
Ma, for *O. centrocarpum* and *S. ramosus*, respectively (Williams et al., 2004), thus providing potential for deep-time pCO$_2$
reconstructions.

Before ε_p values based on dinocysts can used for reconstructing pCO$_2$, several fundamental questions need to be addressed.
Importantly, it remains uncertain whether the CO$_2$ control on ε_p based on controlled growth experiments can be translated to
70 that of the cyst species in the natural environment. In addition, potential offsets in ε_p values between the motile cells and the
cysts need to be established. This is especially important as the cell-cyst relations in carbon isotopes are not necessarily
straightforward, as bulk biomass such as cysts potentially deviates in δ^{13}C values from the various cell components and
potentially not by a constant offset (e.g. Freeman, 2001; Hayes, 2001; Pancost and Pagani, 2006; Schouten et al., 1998; Van
de Waal et al., 2013; Wilkes et al., 2018).

75 We here present the first core-top data for single-species dinocysts in an attempt to constrain the environmental controls on ε_p.
We focus on the species *O. centrocarpum* and compare this data, when possible, to several species of *Spiniferites* (*S. ramosus,
S. mirabilis, S. elongatus*) and *Impagidinium aculeatum*. The environmental relations established are evaluated using simple
models converting carbon isotope fractionation in dinocysts into pCO$_2$ of the surface waters.

2.1 Materials
80 The primary dataset is based on 34 core-top samples (Table 1, Figure 1), collected from the North Atlantic Ocean and
Mediterranean Sea. These samples encompass a substantial natural pCO$_2$ (aq) gradient because the rate of cooling of the North
Atlantic Current exceeds that of CO$_2$ uptake, whereas pCO$_2$ in the Mediterranean is close to or slightly above equilibrium with
the atmosphere. Sample selection is further based on the dinocyst occurrence maps of (Zonneveld et al., 2013), including only
85 samples with an expected relative abundance of at least 10-20% of the target species. Similarly, the coverage of environmental
parameters such as sea surface temperature (SST) and pCO$_2$ and settings was maximized during sample selection. Existing
ocean databases are used to for obtaining the relevant environmental parameters (Table 1).

2.2 Methods
90 Using standard palynological techniques, ca. 5-10 g freeze-dried sediment of the upper 1-2 cm of core material was
processed for each sample. This involved dissolving carbonates and silicate components using strong acids (HCl, 30% and HF
38-40%). After acid steps, residues were pH-neutralized and sieved using an ultrasonic bath and 250 and 10μm nylon mesh
sieve to remove large and small particles, respectively. Subsequently, samples were transferred to glass test tubes with
ultraclean water and centrifuged at 3200 rpm for 10 minutes to obtain an optimum concentrate of the sample material. Prior to
95 dinocyst selection, samples were stored in 4 mL glass vials in milliQ water.

A micro-manipulator consisting of a Leica inverted microscope and a Narishige IM-9B microinjector connected to a strung-out pipette was used to manually select individual dinocysts from a water droplet on a glass petri dish. Dinocyst selection followed a strict protocol, in which cyst morphology (primarily cyst shape and process length) was kept constant and contribution of other organic particles minimized. Specimens with darker coloration or amorphous organic matter adhered to

100 the cyst or processes were avoided. In the case of *O. centrocarpum*, the morphological selection primarily involved selecting specimens of equal size and process length to avoid cysts that may be derived from different environments (e.g. Mertens et al., 2009). For *Spiniferites*, we were able to distinguish and separate three distinct morphological species in sufficient numbers; *S. ramosus*, *S. elongatus* and *S. mirabilis*. For all dinocyst species, the selected diameter excluding processes was in the order of ~30-40 μm, except for *S. mirabilis* (~60 μm), although constraining the exact size of each individual specimen was not feasible

105 within the current analytical procedures. Stable carbon isotope analyses for individual samples are based on replicating the analyses of single of dinocysts, with ~30 individual measurements being conducted to obtain a reasonably precise and accurate (~0.3-0.4‰) sample average (van Roij et al., 2016). Given the size of the dinocysts used here (~30-40 μm cyst diameter), 3-7 specimens were required for each measurement and hence ~150 cysts were required to obtain sample averages (Table 1).

Dinocysts were placed on a 6 mm Ø nickel sample tray, after which an identical second tray is added on top and

110 compressed to fixate the dinocysts. Before placement in the ablation chamber, approximately ~1 mm^2 of International Atomic Energy Agency CH-7 (IAEA-CH7) polyethylene standard (PE; certified $\delta^{13}C$ value −32.151‰ ± 0.050‰; 1σ) was added to the sample tray. Stable carbon isotope analyses of the dinocysts followed the procedures described in previous work (van Roij et al., 2016; Sluijs et al., 2018), utilizing the recently developed Laser Ablation – nano Combustion – Gas Chromatography – Isotope Ratio Mass Spectrometry (LA-nC-GC/IRMS) method. Fragments resulting from deep ultraviolet LA were carried

115 using a continuous Helium flow in 0.32 mm capillaries and oxidized in a combustion oven at 940 ºC. The resultant CO_2 was transported to a GC combustion interface, dried in a nafion tube using a He counterflow and subsequently into a ThermoFisher DeltaV Advantage IRMS for isotope analysis. Each analytical run included 5 standards with signal intensity above 4 Vs (ca. 40 ng C; $\delta^{13}C$ precision better than 0.5‰) to allow calibrating to the Vienna Peedee Belemnite (VPDB) scale. Direct visual monitoring of the ablation process was used as initial quality assessment of each individual measurement.

120

To calculate the fractionation factor ε_p of the dinocysts relative to dissolved inorganic carbon (DIC) in which the dinocyst was produced, we take the $\delta^{13}C_{DIC}$ from the modeled grid of Tagliabue and Bopp (2008). As many dinoflagellate species, including those that produce *O. centrocarpum* and *S. ramosus* cysts, are able to utilize both HCO_3^-, which makes up the majority of DIC, and CO_2 for carbon fixation (Hoins et al., 2016a), we also compare the $\delta^{13}C_{DINO}$ data to $\delta^{13}C_{CO2}$ and with

125 overall sea water carbon partitioning.

ε_{p-DIC} is calculated as: $\delta^{13}C_{DIC} – \delta^{13}C_{DINO}$ and ε_{p-CO2} is calculated as $\delta^{13}C_{CO2} – \delta^{13}C_{DINO}$. For the latter the $\delta^{13}C$ of dissolved CO_2 is calculated from $\delta^{13}C_{DIC}$ using the temperature-dependent fractionation between DIC and $CO_{2(aq)}$ (Mook et al., 1974). To evaluate the dominant contributions to ^{13}C-fractionation in dinocysts, we compare the ε_{p-DIC} and ε_{p-CO2} values to measured and interpolated physicochemical parameters. We test a suite of parameters, $[NO_3]$, $[PO_4]$, $[Si]$, alkalinity, pCO_2,

130 SST and SSS, which are extracted using Ocean Data Viewer (https://data.unep-wcmc.org/) from existing (gridded) datasets (Gouretski and Koltermann, 2004; Takahashi et al., 2014, 2016) (Supplementary Data File). Where possible, data are averaged over a grid 4º longitude and latitude around the sample position. This is both to reduce errors introduced by data scarcity and to account for potential lateral transport of dinocysts during sinking (Nooteboom et al., 2019). Carbonate chemistry is calculated using the R-package seacarb (Gattuso et al., 2019), with alkalinity and pCO_2 as input variables to calculate the
135 other relevant parameters of the carbonate system: the relative contributions of $CO_2(aq)$, HCO_3^- and CO_3^{2-}, i.e. carbon speciation.

Ideally, all environmental parameters would be known for the location and time as the dinoflagellates lived and encysted. This is, however, unfeasible because the core-top sediments integrate cysts from at least the last few decades, but in settings with low accumulation rates, up to centuries. We therefore apply a rough correction for pCO_2 based on the assumption
140 that local air-sea gas exchange has remained similar and apply a correction that equals the atmospheric pCO_2 rise between the measuring date and 1850 AD. While changes in SST, SSS and nutrient concentrations are also expected, partly also induced by anthropogenic activity, trends in these parameters are generally subtle and more complex than for pCO_2 and would require site-specific reconstructions. Recent wide-spread eutrophication and enhanced productivity may impact the carbon isotope results (e.g. by countering the enhanced pCO_2 effects) through increased DIC uptake in algal blooms. However, as
145 eutrophication mainly affected coastal areas (Hallegraeff, 1993; Anderson et al., 2002), this is expected to play a minor factor at our, mostly open marine, sample localities (Figure 1). Lastly, long-term natural changes in nutrients, SSS and SST also occur and it is currently not possible to fully filter out the various anthropogenic offsets. With the exception of pCO_2, we hence assume all parameters (SST, SSS, nutrients) to be constant over the period the core top samples represent.

150 **3. Results**

3.1 Carbon yields from dinocyst analyses

Despite our pre-screening to include only samples with high relative abundance of the target species, some of the selected samples contained too few dinocysts or in too low abundance relative to other organic particles (amorphous organic matter, plant debris, pollen, non-dinocyst marine palynomorphs etc.), to be used in our study. Ultimately, out of the initial sample set
155 of 34 samples, 19 were found suitable for species specific dinocyst stable carbon isotope analyses (Table 1).

Typically, ~150 individual cysts were picked and analyzed for a total of 20-50 measurements, amounting to 3-7 cysts per carbon isotope measurement. We calculate an average signal size of 0.2 Vs for a single cyst, which amounts to a carbon yield of ~6-7 ng C cyst^{-1} (van Roij et al., 2016). Although the variability in signal intensity from individual measurements suggests there is substantial intra-sample (cyst-cyst) variability, no significant offsets in average carbon content per cyst were observed
160 between samples, suggesting the average carbon content of the cysts within each of the analyzed populations is similar. *Spiniferites mirabilis* is the notable exception to this rule, as far fewer specimens of this species are needed for a single $\delta^{13}C_{cyst}$ measurement. Based on the signal intensity per specimen we estimate that this larger cyst species contains twice the amount of C compared to *S. ramosus*, *S. elongatus* and *O. centrocarpum*.

3.2 Carbon isotope measurement data

The 949 individual analyses range in $\delta^{13}C$ from ~ -18.5‰ to -35.5‰. No relation was observed between $\delta^{13}C$ and signal size (Vs), except at the very low end (≤0.2 Vs) (Figure 2), in line with earlier analyses (van Roij et al., 2016). In this low range, the median of the $\delta^{13}C$ values rises from -28‰ below 0.1 Vs to values between -22 and -25‰ above 0.2 Vs. In the ≤0.2 Vs range the $\delta^{13}C$ average of both the cysts and PE converge between -25‰ and -30‰, with substantial scatter. Poorer performance at such low C masses and signal intensities is expected, as these extremely small signal sizes and poor signal to noise ratio (below ~3:1) approach the limit of our method. Consequently, even a very minor contamination source would bias values and result in larger scatter, as also apparent in the PE standard at a similar signal intensity (van Roij et al., 2016; Figure 2). Due to a worsening signal-noise ratio, we find a noticeable degree of $\delta^{13}C$ biasing is likely to occur at signal intensities below 0.2 Vs, and values for the standard and dinocysts converge around -27‰ in this range (Fig. 2A).

Before comparing our data with environmental variables, we therefore assess the impact of a very minor, but consistent, background contamination on the carbon isotope signal at low signal intensities (e.g. Fig. 2A). A constant addition of *ca.* 0.04 Vs (≤ 1 ng C) of a background C source with a $\delta^{13}C$ of -27‰ may explain the positive skewing in the standard PE $\delta^{13}C$. Using a simple isotope end-member / mass balance mixing model to correct for skewing (Fig. 2B), we calculated an average deviation from the measured PE and dinocyst values for intensities below 0.2 Vs in the order of |2.6‰| and |1.3‰|, respectively. The standard deviation of the data increases approximately 3-fold (Figure 2B) compared to the raw measurement data below 0.2 Vs, but remains virtually unchanged above 0.2 Vs and the calculated deviation from the measured value is also much reduced above 0.2 Vs (|<0.3‰|).

The data correction using our simple mixing model eliminates the skew towards -27‰ at low signal intensities, and removes signal size $\delta^{13}C$-dependency below 0.2 Vs for both the isotopically homogeneous PE and the heterogeneous dinocyst data (Figure 2A, B). This suggests our method of bias correction is warranted, but the increased variability at very low intensities and lack of independent control on the exact size and $\delta^{13}C$ of the background contamination implies the data associated with the lowest signal intensities remain significantly less reliable. We therefore apply a hard cut-off, and use only corrected data with a signal size above 0.2 Vs.

The $\delta^{13}C_{DINO}$ is non-normally distributed in many samples and also in different species (Table 1, Figure 3). Distributions have a tendency to be tailed towards lower values. This is not due to analytical error or otherwise related to low signal intensity as we used a 0.2 Vs cut-off to eliminate the worst affected samples (see above) and a minor correction for background C addition was sufficient to eliminate skewing at low signal intensities. The remainder of skewing in the sampled populations thus represents a real signal.

The core-top samples are expected to contain a mixed assemblage of dinocysts produced mostly within the last centuries to millennia, including cysts produced during the last few decades affected by anthropogenic influences. Also the different

seasons are obviously mixed within a single sample. This results in a mixture of cysts representing range of environmental conditions, especially with respect to CO_2 concentrations. To avoid a systematic bias towards the most recent times when

200 atmospheric CO_2 was already elevated above pre-industrial Holocene background (~280 ppmv), cysts produced after the industrial revolution should be avoided from proxy-calibration efforts. Including these cysts would skew the carbon isotope value of organic matter towards more negative values through a combination of the influence of fossil fuel combustion on the $\delta^{13}C$ of atmospheric and surface ocean CO_2 (-2‰ over the last 150 years; (Francey et al., 1999; Keeling et al., 2017) and enhanced carbon isotope fractionation at higher $p CO_2$ in photoautotrophs, including dinoflagellates (Freeman and Hayes, 1992;

205 Pagani, 2013; Hoins et al., 2015). Distinctly non-normally distributed $\delta^{13}C$ values were not previously observed in recent pollen and ancient dinocyst species analyzed with the same method (van Roij et al., 2016; Sluijs et al., 2018). Therefore, a certain influence of Suess-effect and increased $p CO_2$ impacts on the $\delta^{13}C_{DINO}$ data is likely and this contributes to the, predominantly ^{13}C-depleted, outliers and negative skewing of the $\delta^{13}C$ distributions (Figure 3).

To limit both the potential impacts of analytical limitations for the lower yield measurements and offsets due to fossil C input,

210 we conservatively removed measurement outliers from the $\delta^{13}C$ population (outside ±2.5 IQR). This leaves 870 individual $\delta^{13}C_{DINO}$ measurements, 549 for *O. centrocarpum*, 292 for *Spiniferites* (157 *S. ramosus*, 69 *S. elongatus* and 66 *S. mirabilis*) and 29 for *I. aculeatum* (Table 1). We assume these assemblages are representative of ocean conditions prior to the massive increase in anthropogenic carbon emissions.

215 Because most of the omitted data (79 measurements in total) is comparatively ^{13}C-depleted, the resulting $\delta^{13}C$ of the populations are close to statistically indistinguishable from a normal distribution (Shapiro-Wilk $p = 0.05$-0.1) or representative of a normal distribution (Table 1). For practical purposes however, we assume all populations normally distributed for further statistical analyses. We then use the mean carbon isotope value ($\delta^{13}C_{DINO}$) and signal intensity in volt seconds (Vs) of each sample. The standard error of the mean ranges from ~0.2 to 0.7‰ and depends primarily on the number of measurements in

220 cases where n<30, in line with expected values based on replicate measurements of the PE standard (van Roij et al. 2016) (Figure 4).

The range of measured $\delta^{13}C_{DINO}$ values (~5‰) far exceeds the variability in surface ocean $\delta^{13}C_{DIC}$ (~1 ‰) and $\delta^{13}C_{CO2}$ (~2.5‰), implying the increased fractionation likely reflects changing uptake or leakage of different inorganic carbon phases

225 (CO_2 and HCO_3^-; Hoins et al., 2016b), and this determines most of the variability in the $\delta^{13}C_{DINO}$ data.

3.4 Environmental parameters and correlation

The simple (non-weighed) linear regressions show poor correlations between $\varepsilon_{p\text{-}DIC}$ and $\delta^{13}C_{DIC}$ for all environmental parameters, and the correlations improve when compared to $\varepsilon_{p\text{-}CO2}$ (Table 2a, b). However, at face value it seems none of the

230 tested parameters individually explain the majority of the observed variance in $\varepsilon_{p\text{-}DIC}$ (maximum R^2 (~0.1) or $\varepsilon_{p\text{-}CO2}$ (maximum R^2 with $p CO_2$ (~0.45), despite high significance (low p-values) of the regressions. The explained variance increases massively

when e.g. polynomial regressions are applied. Several controlled growth experiments indeed show a non-linear response of ε_p as a function of pCO_2 of the growth medium (Hoins et al., 2015) although the number of data points in such experiments limit full mathematical descriptions of the trends within the pCO_2 range of this field study. Here, a second-order polynomial

235 regression achieves an R^2 of ~0.74 and ~0.79 for the non-weighted and weighted versions, respectively.

It is conceivable that other environmental parameters also significantly contribute to ε_p variability (Fig. 5). For example, $[PO_4]$, $[NO_3]$, and pCO_2 contribute significantly to a (linear) multiple-regression model, which takes the form of $\varepsilon_{p\text{-}CO2} = c + xCO_2 + yPO_4 + zNO_3$, where c, x, y and z are numerical constants. The multiple regression model using these three parameters covers ~58% of the variance in *O. centrocarpum* $\varepsilon_{p\text{-}CO2}$ (p < 0.001, not weighted), and 65% when weighted to number of measurements

240 per sample. Including more parameters, such as SST, oxygen concentrations, or other carbonate system parameters, explains slightly more of the observed variance, but does not significantly improve the model. The residual mean standard error of the CNP-ε_p multiple regression model is ~0.82‰ while a linear regression with only pCO_2 yields 1.05‰. Only weighted regressions given here and reported ranges of the constants represent one standard error. These models have the following optimal formats:

245

Equation 1 linear:

$\varepsilon_{p\text{-}CO2} = 6.7 \pm 1.9 + 0.031 \pm 0.007 \, pCO_2$

(Adjusted R^2 = 0.51, p <0.001, RMSE = 1.05‰) (Figure 5 a)

250 Equation 2 quadratic:

$\varepsilon_{p\text{-}CO2} = 37.9 \pm 6.4 - 0.206 \pm 0.048 \, pCO_2 + 4.43 \times 10^{-4} \pm 8.97 \times 10^{-5} \, pCO_2{}^2$

(Adjusted R^2 = 0.79, p <0.001, RMSE = 0.64‰) (Figure 5 a)

Equation 3a multiple-regression linear:

255 $\varepsilon_{p\text{-}CO2} = 6.4 \pm 2.6 + 0.034 \pm 0.008 \, pCO_2 + 1.11 \pm 0.4 \, NO_3 - 10.0 \pm 3.2 \, PO_4.$

(Adjusted R^2 = 0.65, p < 0.001, RMSE = 0.82‰) (Figure 5 d)

Equation 3b adjusted for application in the paleo-domain:

$\varepsilon_{p\text{-}CO2} = 6.4 \pm 2.6 + 0.034 \pm 0.008 \, pCO_2 - 1.1 \pm 3.2 \, PO_4.$

260

Equation 4 multiple-regression linear:

$\varepsilon_{p\text{-}DIC} = 18.7 \pm 2.6 + 0.024 \pm 0.008 \, pCO_2 + 1.34 \pm 0.4 \, NO_3 - 10.3 \pm 3.2 \, PO_4$

(Adjusted R^2 = 0.47, p = 0.004, RMSE = 0.83‰)

265   The two linear multiple regression models are offset (Equations 3a and 4), primarily as a result of the carbon isotope fractionation between HCO_3 and CO_2. The slope with respect to pCO_2 also varies slightly between the models for $\varepsilon_{p\text{-DIC}}$ and $\varepsilon_{p\text{-CO2}}$ due to the temperature dependent fractionation between HCO_3 and CO_2, but the slopes with NO_3 and PO_4 are indistinguishable. The quadratic regression seemingly better fits the variability observed in $\varepsilon_{p\text{-CO2}}$ compared to other (multiple) linear regressions and removes any structure in the residuals, potentially signaling a non-linear response in $\varepsilon_{p\text{-CO2}}$ to pCO_2. This

270   regression also indicates insensitivity to pCO_2 below ~240 µatm (Figure 5a).

4. Discussion

4.1 Absolute values, comparison to marine organic matter

The recorded $\delta^{13}C_{DINO}$ range and absolute values (~ -18‰ to -35‰) correspond well with global $\delta^{13}C$ values previously

275   reported for marine particulate organic matter ($\delta^{13}C_{POC}$) (e.g. Freeman and Hayes, 1992) and modeled phytoplankton biomass (e.g. Magozzi et al., 2017; Tagliabue and Bopp, 2008). Consequently, $\varepsilon_{p\text{-DIC}}$ and $\varepsilon_{p\text{-CO2}}$ are also within the expected range for general marine particulate organic matter. However, the intra-sample variance of $\delta^{13}C_{DINO}$ appears to be substantial, often spanning most of the full range (~10‰) observed for $\delta^{13}C_{POC}$. Some of the observed variability might be related to the limited analytical precision during measurements of the extremely small amounts of carbon of individual dinocysts. Fully constraining

280   the contribution of this analytical uncertainty to the observed variance is, however, not possible because of unresolvable micrometer-scale heterogeneity in the PE standard (van Roij et al., 2016; Sluijs et al., 2018). In most cases, the variance in $\delta^{13}C_{DINO}$ is similar to that of the standard. Still, it is likely that some of the seasonal $\delta^{13}C_{DIC}$ differences are also recorded in the $\delta^{13}C_{DINO}$, and that some additional inter-specimen $\delta^{13}C$ variance is present. This is to be expected since the $\delta^{13}C$ populations from our integrated core-top samples span seasons, decades and thus also considerable variability in seawater properties and

285   population change. Because we analyzed 3-7 specimens per ablation event, as single-cyst carbon yield (~7 ng C) from these cyst-sizes approached the limit for reliable measurements (van Roij et al., 2016), inter-specimen variability is underestimated. Moreover, we minimized potential influence of differences in cell size or shape through manual selection. We thus analyzed a population where the pre-selection of similar-sized cysts restricts the variance in cell surface area and volume, unlike biomarker-based proxies for which the cell size has to be reconstructed independently (Henderiks and Pagani, 2007; Stoll et

290   al., 2019). This approach could reduce scatter in the relation of ε_p to environmental variables (Popp et al., 1998).

4.2 Cell – cyst offset

One of the striking differences between the here generated data and the existing culture experiments, is that carbon isotope fractionation of dinocysts in the natural environment appears to be much larger than that of motile cells from controlled growth

295   (dilute batch) experiments (Hoins et al., 2015, 2016b). We find average ε_p values ranging between 13-20‰ and 23-29‰ with respect to CO_2 and DIC. Cultured cells of *O. centrocarpum* yielded not only a smaller overall ε_p, but also a smaller range (~8-12 and 18.5-20‰) across a larger CO_2 gradient, implying the cysts have a much steeper fractionation slope with CO_2 compared

to the motile cells. Despite these differences, the average ε_p for *Spiniferites* species (*S. ramosus*, *elongatus* & *mirabilis*) is often somewhat larger than for *O. centrocarpum* (Figure 3). This is consistent with culture experiments that showed larger CO_2-

300 dependency and overall slightly larger ε_p in the motile species *G. spinifera* compared to *P. reticulatum* (Hoins et al., 2015). While the cultured single strains and dinoflagellate populations in nature may behave somewhat differently, we do not expect that this alone underlies such a marked offset between the motile cultured cells and natural cysts. Natural cysts and cultured cells seem consistently offset in $\delta^{13}C$, although at present the exact amplitude of this offset can not be determined. However, such an offset is in line with certain compounds in dinoflagellate cells being depleted in ^{13}C relative to the bulk biomass

305 (Schouten et al., 1998; Wilkes et al., 2017). The organic-walled dinocysts consist of mostly aliphatic and aromatic compounds, forming a complex biopolymer referred to as dinosporin (de Leeuw et al., 2006; Versteegh et al., 2007, 2012). Depending on the biosynthetic pathway of the cyst-material and the derivation or degradation of the original compounds, this may result in offsets in $\delta^{13}C$ values between cysts and the motile cells. A potential additional fractionation might be introduced during taphonomy and also later by the processing of sediments to concentrate the dinocysts from sediment samples. The sediment

310 processing involves hydrochloric and hydrofluoric acids, which affects the more labile organic compounds. Last, it is conceivable that fractionation in the dilute batch experiments may be reduced by e.g. higher-than-natural growth rates. This may be supported by chemostat culture experiments on *Alexandrium tamarense* (Wilkes et al., 2017), which show a (much) greater fractionation compared to the dilute batch experiments (Hoins et al., 2015). Although it concerns a different dinoflagellate species, this may raise the question whether the observations from the dilute batch cultures are representative of

315 natural conditions. The range of options cannot be narrowed down until cultured cysts are compared to their motile cells harvested from the same culture, and treated using similar techniques as the sediments, inferences on the origin and amplitude of the offsets between the cells and cysts of *O. centrocarpum* and *Spiniferites* remain speculative.

4.3 Environmental controls on carbon isotope fractionation

320 Carbon isotope fractionation is determined by RubisCO and several environmental parameters, dominantly pCO$_2$, but also cell size and shape, growth rates and nutrient or light regimes (e.g. Freeman and Hayes, 1992; Pagani, 2013; Popp et al., 1998; Stoll et al., 2019 and many others). In most cases, fractionation is pCO$_2$ dependent, and consequently ε_p in various groups and genera has been used as a paleo-pCO$_2$ proxy (e.g., Freeman and Hayes, 1992; Pagani, 2013; Rae et al., 2021). We performed a broad-spectrum multiple regression analysis to identify environmental factors that contribute significantly to dinocyst ε_p.

325 The most important parameter is pCO$_2$, in line with previous studies (Freeman and Hayes, 1992). A large part of the remaining variability can be attributed to growth rate and ultimately nutrient content, specifically nitrate and phosphate of the surface waters, in line with previous studies on phytoplankton and dinoflagellate carbon isotope fractionation (Popp et al., 1998; Hoins et al., 2016b; Wilkes et al., 2017; Wilkes and Pearson, 2019). We find that pCO$_2$ and ε_p are positively correlated, while NO$_3$ and PO$_4$ are negatively correlated with ε_p (Fig 4).

330   The inclusion of nutrient levels as environmental factors on the carbon isotope fractionation reduces the error in the fit between the measured and modeled fractionation. In the rare cases where paleo-nutrient concentrations are estimated, reconstructions usually cover only $[PO_4]$, implying the $[NO_3]$ in Eq. 3a and 4 has to be approximated from $[PO_4]$. As $[PO_4]$ and $[NO_3]$ are generally well-correlated (typically ~1:10 $[PO_4]$:$[NO_3]$; here ~1:8) in ocean waters, this is relatively straightforward. For application in the paleo-domain however, nutrient ($[PO_4]$) reconstructions may not be available or considered too unreliable

335   to provide meaningful constraints. In specific cases where accurate paleo-$[PO_4]$ estimates or large changes are reconstructed, Eq. 3b may be applied, in which $[NO_3]$ is substituted for $[PO_4]$ in a 1:8 ratio. However, unless there are clear changes in the nutrient regime or sufficient proxy constraints on the nutrient concentrations, we prefer a calibration based exclusively on carbon isotope fractionation and carbonate system parameters, including sea surface temperature to calculate $\delta^{13}C_{CO_2}$ from $\delta^{13}C_{DIC}$, to reconstruct pCO$_2$.

340

4.4 Influence of carbon concentrating mechanisms: CO₂ insensitivity?

As many phototrophs, including dinoflagellates, have mechanisms for concentrating CO_2 near the cell membrane, the sensitivity of carbon isotope fractionation to ambient CO_2 is expected to diminish below a certain concentration (Badger, 2003, 2021; Stoll et al., 2019). This is particularly the case as dinoflagellates utilize type II RubisCO, which has generally poorer

345   performance compared to type I RubisCO at low CO_2 concentrations (Giordano et al., 2005). Indeed, substantial activity of the carboxyl anhydrase (CA) enzyme, which facilitates the conversion of HCO_3^- to CO_2 inside the cell or near the membrane, was observed in numerous dinoflagellate species, including *Lingulodinium* (Lapointe et al., 2008), *Symbiodinium* (Leggat et al., 1999) and the here analysed *Operculodinium* (Ratti et al., 2007). Also here we find a relatively low sensitivity at the lower end of the CO_2 scale. The lower CO_2 values correspond to the northern-most locations, with trends below 240 μatm becoming

350   somewhat obscured, at a minimum ε_p-CO_2 around 13‰ (Fig. 3). However, part of this levelling of the proxy-relationship may reflect the locally higher nutrient concentrations offsetting the higher CO_2. Though growth rates have a clear influence on ε_p in algal groups (Burkhardt et al., 1999), including dinoflagellates (Wilkes et al., 2017), the dilute batch culturing experiments conducted with *P. reticulatum* showed no clear influence of growth rates on ε_p (see also Sec. 4.2). It is also conceivable that higher growth rates influence ε_p indirectly through, for example, seasonally enhanced CO_2 drawdown, resulting in higher $\delta^{13}C$

355   values in the remaining DIC. This effect may be enhanced by the relatively short growing season at the high latitudes. However, in culture experiments at low CO_2 concentrations with other dinoflagellate species, ^{13}C-fractionation was higher under nutrient limiting conditions than under replete conditions (Hoins et al., 2016b). Because of these confounding factors, the influence of carbon concentrating mechanisms on ε_p in *O. centrocarpum* is difficult to gauge with the presently available data, and would ideally be tested using high nutrient or very low CO_2 concentrations.

360   Still, also in the relatively limited range the current ocean offers for testing pCO$_2$ proxies we have established a robust, albeit not overly sensitive, relation between pCO$_2$ and dinocyst $\delta^{13}C$. Our cyst-based calibration yields more conservative and arguably more realistic absolute CO_2 estimates and variability compared to available culture-based calibrations as it is based

on the same compounds as will be analyzed in the paleo-domain. The low-sensitivity at low CO_2 implies that, until better constraints become available, the proposed calibration is less suitable for application during the Pleistocene glacials. While

365 our data does not preclude fractionation smaller than the here observed minimum (~13‰) during low pCO_2 periods, increased sensitivity at higher CO_2 suggests that CO_2 above 240 µatm can be reconstructed with reasonable precision.

5. Conclusions - Proxy potential, limitation and calibrations

Our new modern ocean single-species carbon isotope fractionation dataset shows promising trends with environmental

370 variables, pCO_2 and nutrients. The selection of individual cysts allows control of cell size and species, which reduces uncertainty in proxy calibration and application compared to approaches based on organic substrates which inevitably integrate entire communities. Still, many of the challenges associated with other proxies based on organic substrates are encountered here as well. For example, we observed an impact of nutrients on carbon isotope fractionation, likely related to differences in growth rates. Similarly, at low pCO_2 values sensitivity is reduced, possibly as a result of carbon concentrating mechanisms

375 involved in dinoflagellate C uptake. Another remaining challenge is the observed difference between the cultured populations and cysts from the core top sediments. This is a pronounced difference, not only in the absolute isotope fractionation values but also in the slope of the CO_2 sensitivity, which appears to be much larger for the cysts and requires attention in future culture studies.

The offset in $\delta^{13}C$, combined with uncertainties in fractionation between the motile cells and dinocysts imply that CO_2

380 reconstructions using culture-based calibrations are more likely to overestimate past pCO_2. Furthermore, the large spread in our data (~5‰ between high and low CO_2) suggests that, due to this high sensitivity in the cysts, the method is also suited to study population dynamics.

Data availability

385 All newly generated data will be uploaded to a permanent online repository (pangaea.de) upon publication.

Author contribution

AS & GJR designed the study, LvR, IK & JF processed samples, generated and analysed data, JF wrote the original draft, AS & GJR reviewed and edited the manuscript. AS acquired funding for this study.

390

Competing interests

The authors declare that they have no conflict of interest.

Acknowledgments

395 We thank A. van Dijk, M. Kienhuis and H. de Waard (Utrecht University) for technical and analytical assistance. AS acknowledges funding from Netherlands Organisation for Scientific Research (NWO) #ALWOP.223 and European Research Council (ERC) Starting grant #259627. This work was carried out under the program of the Netherlands Earth System Science Centre (NESSC), financially supported by the Dutch Ministry of Education, Culture and Science.

References

Anderson, D. M., Glibert, P. M. and Burkholder, J. M.: Harmful algal blooms and eutrophication: Nutrient sources, composition, and consequences, Estuaries, 25(4), 704–726, doi:10.1007/BF02804901, 2002.

Badger, M.: The roles of carbonic anhydrases in photosynthetic CO2 concentrating mechanisms, Photosynth. Res., 77(2–3), 83–94, doi:10.1023/A:1025821717773, 2003.

Badger, M. P. S.: Alkenone isotopes show evidence of active carbon concentrating mechanisms in coccolithophores as aqueous carbon dioxide concentrations fall below 7 μmolL-1, Biogeosciences, 18(3), 1149–1160, doi:10.5194/bg-18-1149-2021, 2021.

Barnola, J. M., Raynaud, D., Korotkevich, Y. S. and Lorius, C.: Vostok ice core provides 160,000-year record of atmospheric CO2, Nature, 329(6138), 408–414, doi:10.1038/329408a0, 1987.

Bijl, P. K., Houben, A. J. P., Schouten, S., Bohaty, S. M., Sluijs, A., Reichart, G.-J., Damsté, J. S. S. and Brinkhuis, H.: Transient Middle Eocene Atmospheric CO2 and Temperature Variations, Science., 330(6005), 819–821, doi:10.1126/science.1193654, 2010.

Boller, A. J., Thomas, P. J., Cavanaugh, C. M. and Scott, K. M.: Low stable carbon isotope fractionation by coccolithophore RubisCO, Geochim. Cosmochim. Acta, 75(22), 7200–7207, doi:10.1016/j.gca.2011.08.031, 2011.

Boller, A. J., Thomas, P. J., Cavanaugh, C. M. and Scott, K. M.: Isotopic discrimination and kinetic parameters of RubisCO from the marine bloom-forming diatom, Skeletonema costatum, Geobiology, 13(1), 33–43, doi:10.1111/gbi.12112, 2015.

Burkhardt, S., Riesebell, U. and Zondervan, I.: Effects of growth rate , CO 2 concentration , and cell size on the stable carbon isotope fractionation in marine phytoplankton, Geochim. Cosmochim. Acta, 63(22), 3729–3741, 1999.

Eberlein, T., Van de Waal, D., Brandenburg, K., John, U., Voss, M., Achterberg, E. and Rost, B.: Interactive effects of ocean acidification and nitrogen limitation on two bloom-forming dinoflagellate species, Mar. Ecol. Prog. Ser., 543, 127–140, doi:10.3354/meps11568, 2016.

Evitt, W. R.: Sporopollenin dinoflagellate cysts: their morphology and interpretation, Amer Assn of Stratigraphic., 1985.

Farquhar, G. D., Ehleringer, J. R. and Hubick, K. T.: Discrimination and Photosynthesis, 1989.

Fensome, R. A., MacRae, R. A., Moldowan, J. M., Taylor, F. J. R. and Williams, G. L.: The early Mesozoic radiation of dinoflagellates, Paleobiology, 329–338, 1996.

Francey, R. J., Allison, C. E., Etheridge, D. M., Trudinger, C. M., Enting, I. G., Leuenberger, M., Langenfelds, R. L., Michel, E. and Steele, L. P.: A 1000-year high precision record of δ13C in atmospheric CO2, Tellus, Ser. B Chem. Phys. Meteorol., 51(2), 170–193, doi:10.1034/j.1600-0889.1999.t01-1-00005.x, 1999.

Freeman, K. H.: Isotopic biogeochemistry of marine organic carbon, Rev. Mineral. Geochemistry, 43, 579–605,

doi:10.2138/gsrmg.43.1.579, 2001.

430   Freeman, K. H. and Hayes, J. M.: Fractionation of carbon isotopes by phytoplankton and estimates of ancient CO2 levels, Global Biogeochem. Cycles, 6(2), 185–198, 1992.

Frieling, J. and Sluijs, A.: Towards quantitative environmental reconstructions from ancient non-analogue microfossil assemblages: Ecological preferences of Paleocene – Eocene dinoflagellates, Earth-Science Rev., 185(August), 956–973, doi:10.1016/j.earscirev.2018.08.014, 2018.

435   Gattuso, J. P., Epitalon, J. M., Lavigne, H. and Orr, J.: seacarb: Seawater carbonate chemistry. R package version 3.2. 12., n.d.

Giordano, M., Beardall, J. and Raven, J. A.: CO2 Concentrating Mechanisms in Algae: Mechanisms, Environmental Modulation, and Evolution, Annu. Rev. Plant Biol., 56(1), 99–131, doi:10.1146/annurev.arplant.56.032604.144052, 2005.

Gouretski, V. V. and Koltermann, K. P.: WOCE Global Hydrographic Climatology, Berichte des Bundesamtes fur Seeschifffahrt und Hydrogr., doi:10.5065/GS51-V170, 2004.

440   Hallegraeff, G. M.: A review of harmful algal blooms and their apparent global increase*, Phycologia, 32(2), 79–99, doi:10.2216/i0031-8884-32-2-79.1, 1993.

Hayes, J. M.: Fractionation of Carbon and Hydrogen Isotopes in Biosynthetic Processes, Rev. Mineral. Geochemistry, 43(1), 225–277, doi:10.2138/gsrmg.43.1.225, 2001.

Head, M. J.: Modern dinoflagellate cysts and their biological affinities, Palynol. Princ. Appl., 3, 1197–1248, 1996.

445   Henderiks, J. and Pagani, M.: Refining ancient carbon dioxide estimates: Significance of coccolithophore cell size for alkenone-based p CO 2 records, Paleoceanography, 22(3), n/a-n/a, doi:10.1029/2006PA001399, 2007.

Hoins, M., Van de Waal, D. B., Eberlein, T., Reichart, G.-J., Rost, B. and Sluijs, A.: Stable carbon isotope fractionation of organic cyst-forming dinoflagellates: Evaluating the potential for a CO2 proxy, Geochim. Cosmochim. Acta, 160, 267–276, doi:10.1016/j.gca.2015.04.001, 2015.

450   Hoins, M., Eberlein, T., Van de Waal, D. B., Sluijs, A., Reichart, G.-J. and Rost, B.: CO2-dependent carbon isotope fractionation in dinoflagellates relates to their inorganic carbon fluxes, J. Exp. Mar. Bio. Ecol., 481, 9–14, doi:10.1016/j.jembe.2016.04.001, 2016a.

Hoins, M., Eberlein, T., Groβmann, C. H., Brandenburg, K., Reichart, G.-J., Rost, B., Sluijs, A. and Van de Waal, D. B.: Combined Effects of Ocean Acidification and Light or Nitrogen Availabilities on 13C Fractionation in Marine Dinoflagellates,

455   PLoS One, 11(5), e0154370, doi:10.1371/journal.pone.0154370, 2016b.

IPCC: Climate Change 2014: Synthesis Report. Contribution of Working Groups I, II and III to the Fifth Assessment Report of the Intergovernmental Panel on Climate Change, 2014.

Keeling, R. F., Graven, H. D., Welp, L. R., Resplandy, L., Bi, J., Piper, S. C., Sun, Y., Bollenbacher, A. and Meijer, H. A. J.: Atmospheric evidence for a global secular increase in carbon isotopic discrimination of land photosynthesis, Proc. Natl. Acad.

460   Sci. U. S. A., 114(39), 10361–10366, doi:10.1073/pnas.1619240114, 2017.

Kodrans-Nsiah, M., De Lange, G. J. and Zonneveld, K. A. F.: A natural exposure experiment on short-term species-selective aerobic degradation of dinoflagellate cysts, Rev. Palaeobot. Palynol., 152(1), 32–39, 2008.

Lapointe, M., MacKenzie, T. D. B. and Morse, D.: An external δ-carbonic anhydrase in a free-living marine dinoflagellate may circumvent diffusion-limited carbon acquisition, Plant Physiol., 147(3), 1427–1436, doi:10.1104/pp.108.117077, 2008.

465 de Leeuw, J. W., Versteegh, G. J. M. and van Bergen, P. F.: Biomacromolecules of Algae and Plants and their Fossil Analogues, Plant Ecol., 182(1–2), 209–233, doi:10.1007/s11258-005-9027-x, 2006.

Leggat, W., Badger, M. R. and Yellowlees, D.: Evidence for an inorganic carbon-concentrating mechanism in the symbiotic dinoflagellate Symbiodinium sp., Plant Physiol., 121(4), 1247–1255, doi:10.1104/pp.121.4.1247, 1999.

Magozzi, S., Yool, A., Vander Zanden, H. B., Wunder, M. B. and Trueman, C. N.: Using ocean models to predict spatial and

470 temporal variation in marine carbon isotopes, Ecosphere, 8(5), e01763, doi:10.1002/ecs2.1763, 2017.

Mertens, K. N., Ribeiro, S., Bouimetarhan, I., Caner, H., Combourieu Nebout, N., Dale, B., De Vernal, A., Ellegaard, M., Filipova, M., Godhe, A., Goubert, E., Grøsfjeld, K., Holzwarth, U., Kotthoff, U., Leroy, S. A. G., Londeix, L., Marret, F., Matsuoka, K., Mudie, P. J., Naudts, L., Peña-Manjarrez, J. L., Persson, A., Popescu, S. M., Pospelova, V., Sangiorgi, F., van der Meer, M. T. J., Vink, A., Zonneveld, K. A. F., Vercauteren, D., Vlassenbroeck, J., Louwye, S., Nebout, N. C., Dale, B.,

475 De Vernal, A., Ellegaard, M., Filipova, M. and Godhe, A.: Process length variation in cysts of a dinoflagellate, Lingulodinium machaerophorum, in surface sediments: investigating its potential as salinity proxy, Mar. Micropaleontol., 70(1), 54–69, doi:10.1016/j.marmicro.2008.10.004, 2009.

Mook, W. G., Bommerson, J. C. and Staverman, W. H.: Carbon isotope fractionation between dissolved bicarbonate and gaseous carbon dioxide, Earth Planet. Sci. Lett., 22(2), 169–176, doi:10.1016/0012-821X(74)90078-8, 1974.

480 Naafs, B. D. A., Castro, J. M., De Gea, G. A., Quijano, M. L., Schmidt, D. N. and Pancost, R. D.: Gradual and sustained carbon dioxide release during Aptian Oceanic Anoxic Event 1a, Nat. Geosci., 9(2), 135–139, doi:10.1038/ngeo2627, 2016.

Nooteboom, P. D., Bijl, P. K., van Sebille, E., von der Heydt, A. S. and Dijkstra, H. A.: Transport bias by ocean currents in sedimentary microplankton assemblages: Implications for paleoceanographic reconstructions, Paleoceanogr. Paleoclimatology, doi:10.1029/2019PA003606, 2019.

485 Pagani, M.: Biomarker-Based Inferences of Past Climate: The Alkenone pCO2 Proxy, 2nd ed., Elsevier Ltd., 2013.

Pagani, M., Liu, Z., LaRiviere, J. and Ravelo, A. C.: High Earth-system climate sensitivity determined from Pliocene carbon dioxide concentrations, Nat. Geosci., 3(1), 27–30, doi:10.1038/ngeo724, 2010.

Pagani, M., Huber, M., Liu, Z., Bohaty, S. M., Henderiks, J., Sijp, W. P., Krishnan, S. and DeConto, R. M.: The Role of Carbon Dioxide During the Onset of Antarctic Glaciation, Science (80-.)., 334, 1261–1265, doi:10.1126/science.1203909,

490 2011.

PALAEOSENS: Making sense of palaeoclimate sensitivity, Nature, 491(7426), 683–691, doi:10.1038/nature11574, 2012.

Pancost, R. D. and Pagani, M.: Controls on the carbon isotopic compositions of lipids in marine environments, Handb. Environ. Chem. Vol. 2 React. Process., 2 N(October 2005), 209–249, doi:10.1007/698_2_007, 2006.

Popp, B. N., Laws, E. A., Bidigare, R. R., Dore, J. E., Hanson, K. L. and Wakeham, S. G.: Effect of Phytoplankton Cell

495 Geometry on Carbon Isotopic Fractionation, Geochim. Cosmochim. Acta, 62(1), 69–77, doi:10.1016/S0016-7037(97)00333-5, 1998.

Rae, J. W. B., Zhang, Y. G., Liu, X., Foster, G. L., Stoll, H. M. and Whiteford, R. D. M.: Atmospheric CO 2 over the Past 66 Million Years from Marine Archives , Annu. Rev. Earth Planet. Sci., 49(1), 599–631, doi:10.1146/annurev-earth-082420-063026, 2021.

500 Ratti, S., Giordano, M. and Morse, D.: CO2-concentrating mechanisms of the potentially toxic dinoflagellate Protoceratium reticulatum (Dinophyceae, Gonyaulacales), J. Phycol., 43(4), 693–701, doi:10.1111/j.1529-8817.2007.00368.x, 2007.

Roeske, C. A. and O'Leary, M. H.: Carbon isotope effects on enzyme-catalyzed carboxylation of ribulose bisphosphate, Biochemistry, 23(25), 6275–6284, doi:10.1021/bi00320a058, 1984.

van Roij, L., Sluijs, A., Laks, J. J. and Reichart, G.-J.: Stable carbon isotope analyses of ng quantities of particulate organic
505 carbon (pollen) with laser ablation nano combustion gas chromatography isotope ratio mass spectrometry, Rapid Commun. Mass Spectrom., (October 2016), 47–58, doi:10.1002/rcm.7769, 2016.

Rost, B., Richter, K.-U., Riesebell, U. and Hansen, P. J.: Inorganic carbon acquisition in red tide dinoflagellates, Plant, Cell Environ., 29(5), 810–822, doi:10.1111/j.1365-3040.2005.01450.x, 2006.

Schoon, P. L., Sluijs, A., Sinninghe Damsté, J. S. and Schouten, S.: Stable carbon isotope patterns of marine biomarker lipids
510 in the Arctic Ocean during Eocene Thermal Maximum 2, Paleoceanography, 26(3), doi:10.1029/2010PA002028, 2011.

Schouten, S., Klein Breteler, W. C. ., Blokker, P., Schogt, N., Rijpstra, W. I. C., Grice, K., Baas, M. and Sinninghe Damsté, J. S.: Biosynthetic effects on the stable carbon isotopic compositions of algal lipids: implications for deciphering the carbon isotopic biomarker record, Geochim. Cosmochim. Acta, 62(8), 1397–1406, doi:10.1016/S0016-7037(98)00076-3, 1998.

Sluijs, A., van Roij, L., Frieling, J., Laks, J. and Reichart, G.-J.: Single-species dinoflagellate cyst carbon isotope ecology
515 across the Paleocene-Eocene Thermal Maximum, Geology, 46(1), 79–82, doi:10.1130/G39598.1, 2018.

Stoll, H. M., Guitian, J., Hernandez-Almeida, I., Mejia, L. M., Phelps, S., Polissar, P., Rosenthal, Y., Zhang, H. and Ziveri, P.: Upregulation of phytoplankton carbon concentrating mechanisms during low CO2 glacial periods and implications for the phytoplankton pCO2 proxy, Quat. Sci. Rev., 208, 1–20, doi:10.1016/j.quascirev.2019.01.012, 2019.

Tagliabue, A. and Bopp, L.: Towards understanding global variability in ocean carbon-13, Global Biogeochem. Cycles, 22(1),
520 1–13, doi:10.1029/2007GB003037, 2008.

Takahashi, T., Sutherland, S. C., Chipman, D. W., Goddard, J. G., Ho, C., Newberger, T., Sweeney, C. and Munro, D. R.: Climatological distributions of pH, pCO2, total CO2, alkalinity, and CaCO3 saturation in the global surface ocean, and temporal changes at selected locations, Mar. Chem., 164, 95–125, doi:10.1016/j.marchem.2014.06.004, 2014.

Takahashi, T., Sutherland, S. C. and Kozyr, A.: Global Ocean Surface Water Partial Pressure of CO2 Database: Measurements
525 Performed During 1957-2015 (Version 2015), Carbon Dioxide Information Analysis Center, Oak Ridge National Laboratory, U.S. Department of Energy, Oak Ridge, Tennessee., n.d.

Versteegh, G. J. M., Blokker, P., Marshall, C. and Pross, J.: Macromolecular composition of the dinoflagellate cyst Thalassiphora pelagica (Oligocene, SW Germany), Org. Geochem., 38(10), 1643–1656, doi:10.1016/j.orggeochem.2007.06.007, 2007.

530 Versteegh, G. J. M., Blokker, P., Bogus, K., Harding, I. C., Lewis, J., Oltmanns, S., Rochon, A. and Zonneveld, K. A. F.: Infra

red spectroscopy, flash pyrolysis, thermally assisted hydrolysis and methylation (THM) in the presence of tetramethylammonium hydroxide (TMAH) of cultured and sediment-derived Lingulodinium polyedrum (Dinoflagellata) cyst walls, Org. Geochem., 43, 92–102, doi:10.1016/j.orggeochem.2011.10.007, 2012.

Van de Waal, D. B., John, U., Ziveri, P., Reichart, G.-J., Hoins, M., Sluijs, A. and Rost, B.: Ocean Acidification Reduces
535 Growth and Calcification in a Marine Dinoflagellate, PLoS One, 8(6), doi:10.1371/journal.pone.0065987, 2013.

Wall, D. and Dale, B.: "Living fossils" in Western Atlantic plankton, Nature, 211(5053), 1025–1026, 1966.

Wilkes, E. B. and Pearson, A.: A general model for carbon isotopes in red-lineage phytoplankton: Interplay between unidirectional processes and fractionation by RubisCO, Geochim. Cosmochim. Acta, 265, 163–181, doi:10.1016/j.gca.2019.08.043, 2019.

540 Wilkes, E. B., Carter, S. J. and Pearson, A.: CO 2 -dependent carbon isotope fractionation in the dinoflagellate Alexandrium tamarense, Geochim. Cosmochim. Acta, 212, 48–61, doi:10.1016/j.gca.2017.05.037, 2017.

Wilkes, E. B., Lee, R. B. Y., McClelland, H. L. O., Rickaby, R. E. M. and Pearson, A.: Carbon isotope ratios of coccolith–associated polysaccharides of Emiliania huxleyi as a function of growth rate and CO2 concentration, Org. Geochem., 119, 1–10, doi:10.1016/j.orggeochem.2018.02.006, 2018.

545 Williams, G. L., Brinkhuis, H., Pearce, M. A., Fensome, R. A. and Weegink, J. W.: Southern Ocean and global dinoflagellate cyst events compared: index events for the Late Cretaceous–Neogene, in Proceedings of the Ocean Drilling Program, Scientific Results, vol. 189, pp. 1–98., 2004.

Witkowski, C. R., Weijers, J. W. H., Blais, B., Schouten, S. and Sinninghe Damsté, J. S.: Molecular fossils from phytoplankton reveal secular P co 2 trend over the Phanerozoic, Sci. Adv., 4(11), eaat4556, doi:10.1126/sciadv.aat4556, 2018.

550 Zonneveld, K. A. f., Gray, D. D., Kuhn, G. and Versteegh, G. J. m.: Postdepositional aerobic and anaerobic particulate organic matter degradation succession reflected by dinoflagellate cysts: The Madeira Abyssal Plain revisited, Mar. Geol., 408, 87–109, doi:10.1016/j.margeo.2018.11.010, 2019.

Zonneveld, K. A. F., Versteegh, G. J. M. and De Lange, G. J.: Preservation of organic-walled dinoflagellate cysts in different oxygen regimes: a 10,000 year natural experiment, Mar. Micropaleontol., 29(3), 393–405, 1997.

555 Zonneveld, K. A. F., Marret, F., Versteegh, G. J. M., Bogus, K., Bonnet, S., Bouimetarhan, I., Crouch, E., de Vernal, A., Elshanawany, R., Edwards, L., Esper, O., Forke, S., Grøsfjeld, K., Henry, M., Holzwarth, U., Kielt, J.-F., Kim, S.-Y., Ladouceur, S., Ledu, D., Chen, L., Limoges, A., Londeix, L., Lu, S.-H., Mahmoud, M. S., Marino, G., Matsouka, K., Matthiessen, J., Mildenhal, D. C., Mudie, P., Neil, H. L., Pospelova, V., Qi, Y., Radi, T., Richerol, T., Rochon, A., Sangiorgi, F., Solignac, S., Turon, J.-L., Verleye, T., Wang, Y., Wang, Z. and Young, M.: Atlas of modern dinoflagellate cyst distribution
560 based on 2405 data points, Rev. Palaeobot. Palynol., 191, 1–197, doi:10.1016/j.revpalbo.2012.08.003, 2013.
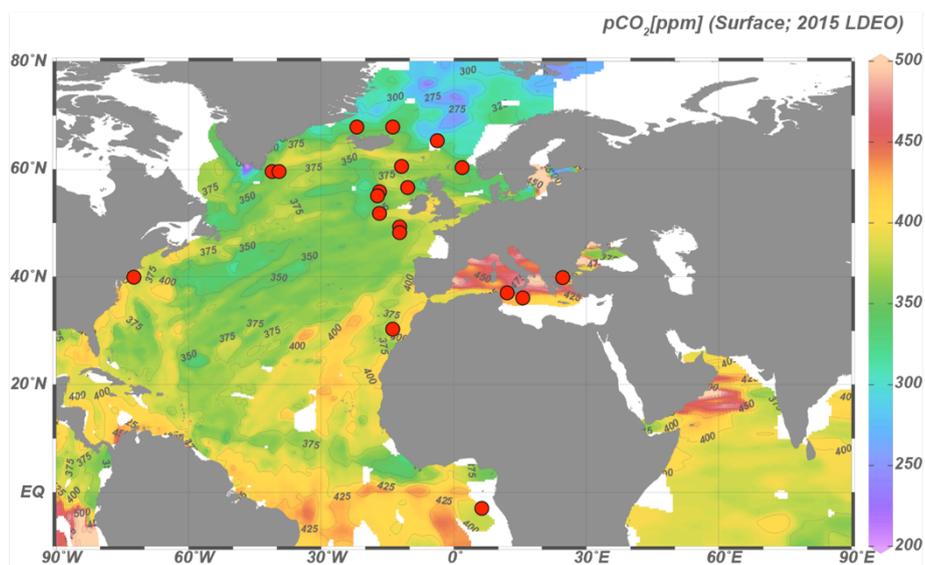
Figure 1. Locations of samples with sufficient *Operculodinium centrocarpum* and/or *Spiniferites* spp.
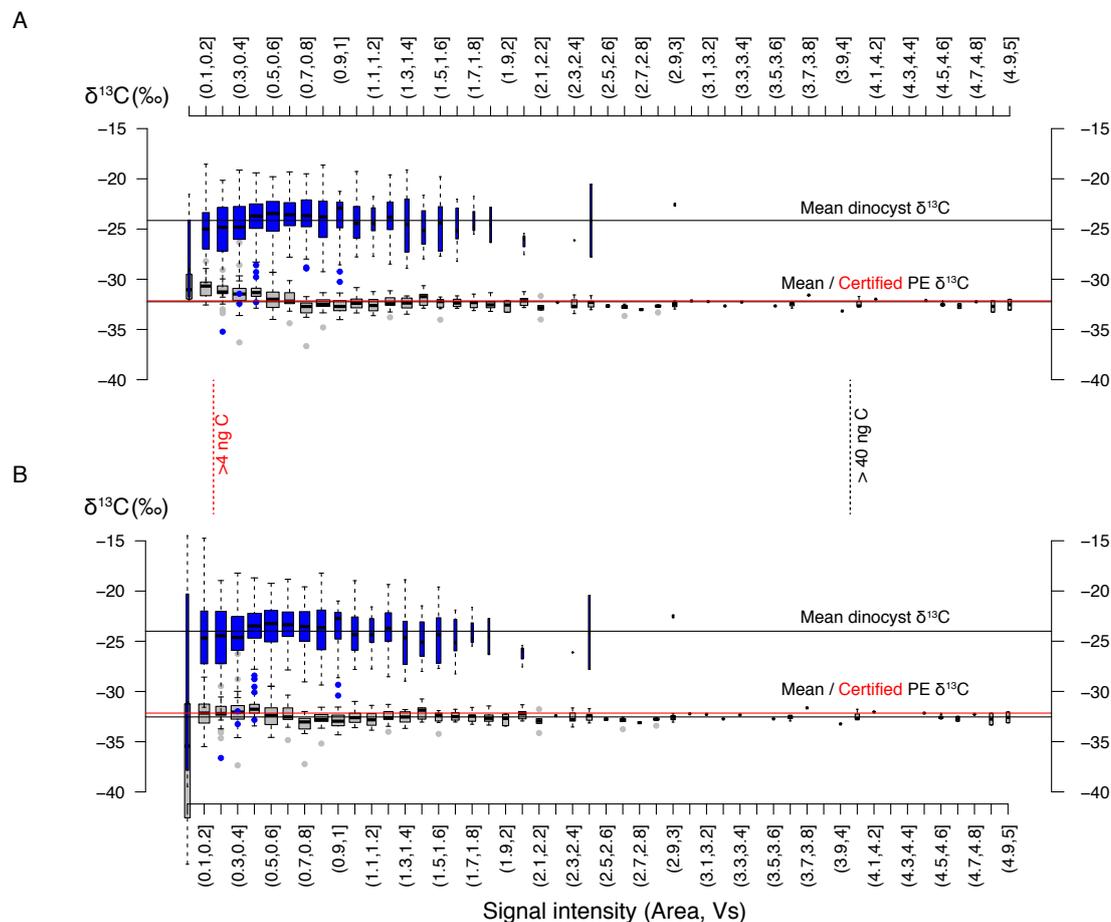
Figure 2. Signal intensity in Volt seconds (Vs) versus carbon isotope value distribution within bins of 0.1 Vs. A. The blue boxplots represent our new dinocyst δ¹³C, and the gray boxplots represent the previously published data for the PE standard (δ¹³C value −32.151‰ ± 0.050‰; 1σ). **B.** Same as A. but for background-corrected values (see §3.2). The vertical black and red line represent cut-off values for individual PE standard measurements (>4 Vs; ~42 ng C; 0.5‰ precision) and individual cyst measurements (>0.2 Vs; ~6 ng C), respectively. The width of each boxplot is square-root scaled with the number of measurements in the respective bins. Note that several bins at the high-end do not contain any data.
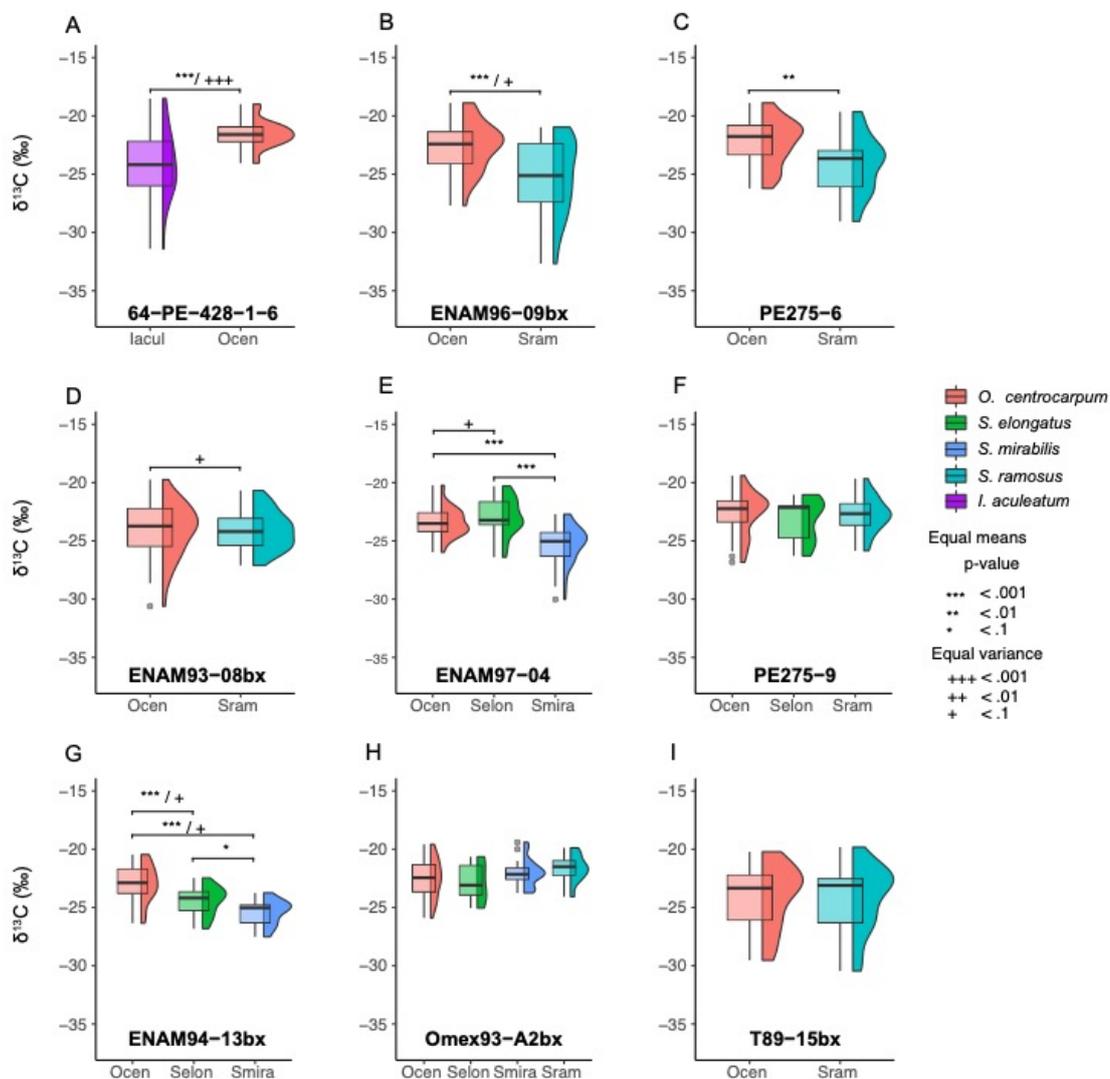
Figure 3. Carbon isotope measurements for multiple species; each panel represents a single sample after eliminating extremely
small measurements sizes (<0.2 Vs), background correction and removing outliers (± 2.5 interquartile range) (paragraph §3.2).
Each box-whisker and δ¹³C distribution plot represents a set of measurements for a single species at their respective locality;
note that tailing towards negative δ¹³C is common.
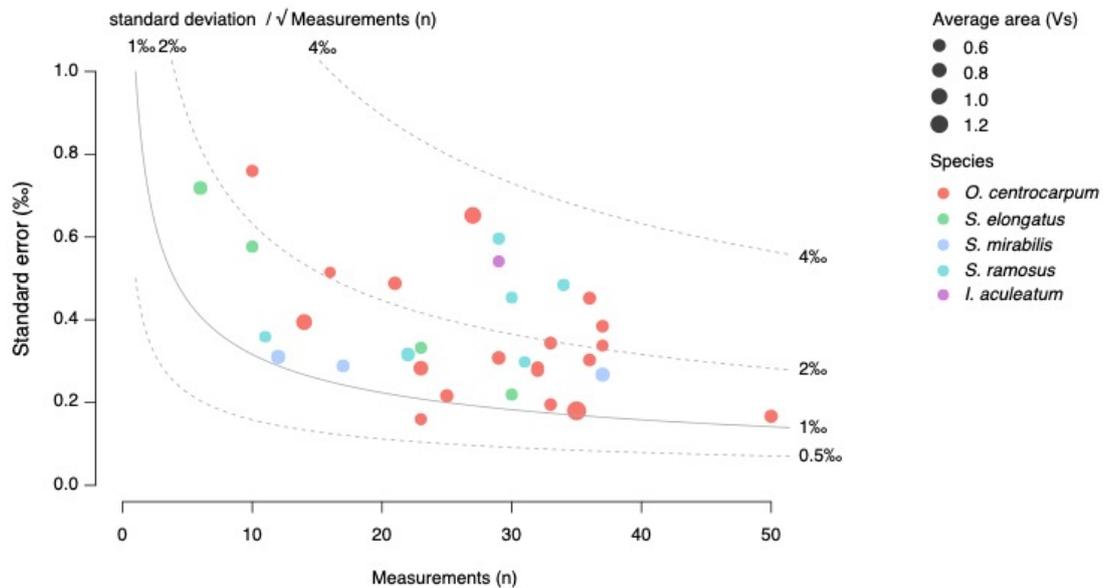
Figure 4. Relation of standard error of $\delta^{13}C_{DINO}$ (‰) with the number of measurements and signal intensity (area in Volt
580   seconds (Vs)). Colors correspond to the various analyzed species.
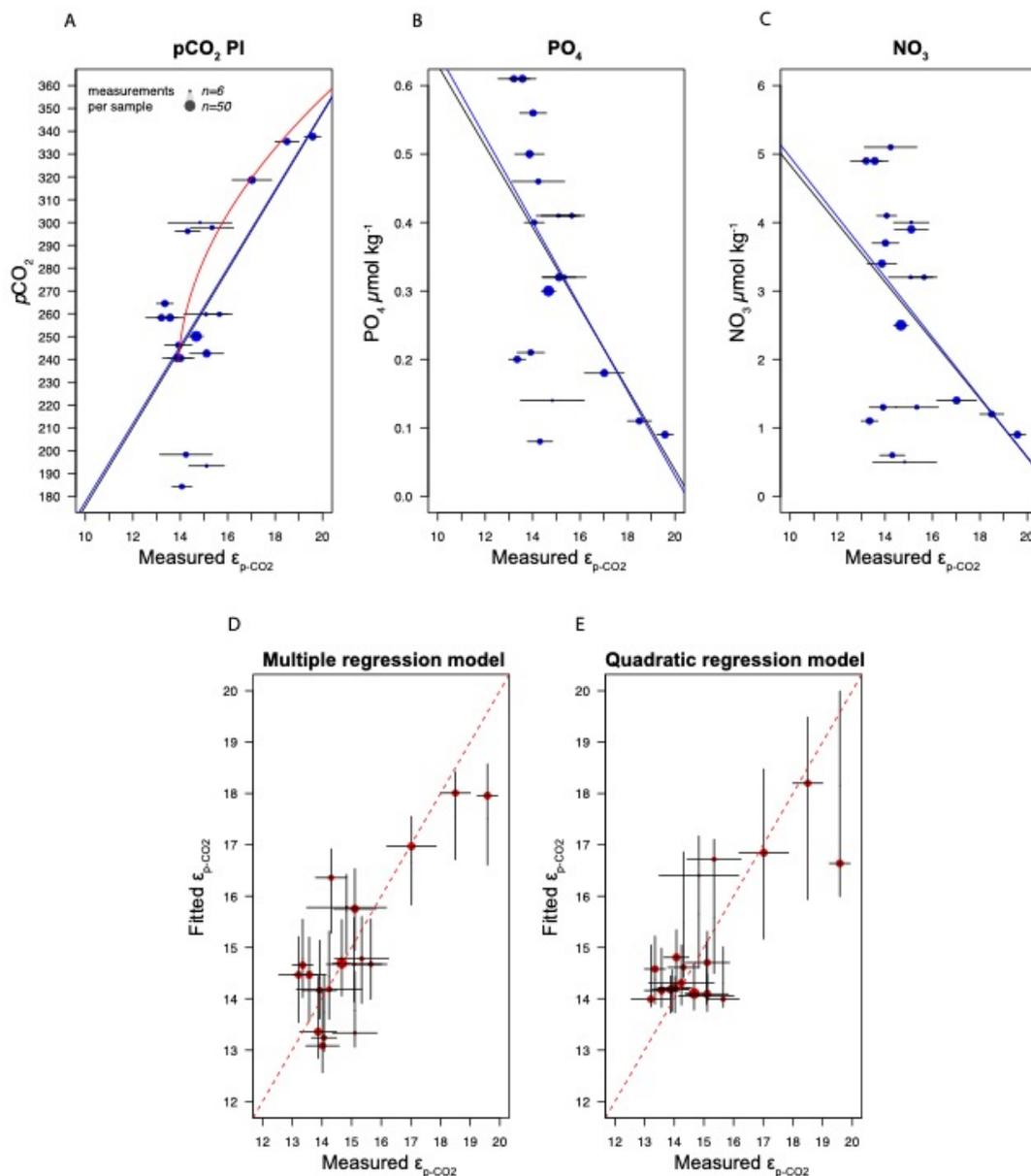
Figure 5. Regression analyses for $\varepsilon_{p\text{-}CO2}$ of *O. centrocarpum* relative to (a) pCO_2 (measured, corrected to pre-industrial values); black line represents simple linear regression, blue lines represent weighted linear regressions and red line (a) represents weighted quadratic regression, (b) phosphate concentrations (PO_4), (c) nitrate concentrations (NO_3). (d) Fitted values illustrating the multiple regression model performance using parameters a-c relative to measured $\varepsilon_{p\text{-}CO2}$. (e) Fitted values using only pre-industrial pCO_2, but applying a quadratic regression (red curve in panel a). Errors on the fitted values in panels d and e from Monte-Carlo simulations (n=1000) for regression models. Symbol size (top left corner of panel a) represents the number of measurements within each sample.

Core-ID	Latitude (°N)	Longitude (°E)	Species	Measurements (n)	S-W normality
NF2012-091	37.977402	-73.669403	*O.centrocarpum*	22 (21)	* ()
PE360-24	55.496231	-15.800755	*O.centrocarpum*	24 (23)	** ()
PE360-45	55.539398	-15.8453	*O.centrocarpum*	23 (16)	()
NA87-02	64.480003	-5.83	*O.centrocarpum*	20 (14)	*** ()
LCD13	67.501282	-15.069252	*O.centrocarpum*	25 (25)	()
LCD10A	66.677437	-24.179598	*O.centrocarpum*	29 (27)	()
MedSea (MC-613)	35.8575	14.105556	*O.centrocarpum*	35 (35)	()
MedSea (MC-614)	35.8075	12.998056	*O.centrocarpum*	33 (32)	* ()
MedSea (MC-645)	40.2175	25.244167	*O.centrocarpum*	33 (23)	** ()
ENAM93-08bx	59.501667	3.69	*O.centrocarpum*	38 (37)	*()
			S.ramosus	33 (32)	()
ENAM94-13bx	60.249997	-11.19	*O.centrocarpum*	36 (33)	()
			S.elongatus	34 (30)	*** ()
			S.mirabilis	13 (12)	()
ENAM96-09bx	57.159917	-10.26	*O.centrocarpum*	39 (37)	()
			S.ramosus	30 (29)	()
ENAM97-04	52.410386	-14.94	*O.centrocarpum*	52 (50)	()
			S.elongatus	23 (23)	()
			S.mirabilis	38 (37)	** (*)
Omex93-A2 bx	49.483	-11.13	*O.centrocarpum*	30 (29)	()
			S.ramosus	13 (11)	*()
			S.elongatus	6 (6)	()
			S.mirabilis	18 (17)	()
PE275-6	59.272369	-38.36	*O.centrocarpum*	34 (33)	*()
			S.ramosus	34 (30)	**()
PE275-9	59.272369	-38.36	*O.centrocarpum*	37 (36)	*(*)
			S.ramosus	23 (22)	*(*)
			S.elongatus	12 (10)	*(*)
T89-15bx	-4.199372	10.05	*O.centrocarpum*	36 (36)	* (*)
			S.ramosus	35 (34)	* (*)
64PE428-1-1-6	47.079782	-10.197305	*O.centrocarpum*	35 (33)	()
			I.aculeatum	30 (29)	()
64PE428-1-6-6	30.67917	-11.930478	*O.centrocarpum*	11 (10)	()

590

Table 1. Core localities, analyzed species, number of measurements and normality of the carbon isotope data. Number
of measurements total and in parentheses measurements used for environmental comparisons (see also results §3.4). Shapiro-

Wilk (S-W) normality test on data: non-normal data distributions are indicated where p values are < 0.1 (*), <0.01 (**) and <0.001 (***), in parentheses the same for the data used for environmental comparisons.

595

Table 2a: Multiple linear regression for all samples where *O. centrocarpum* was analyzed (n = 19), with $\varepsilon_{p\text{-}CO2}$ as dependent variable. Parameters with p-values <0.05 in bold.

	Coeff.	Std.err.	t	p	R^2
Constant	120.0	60.2	1.992	0.093	
CO_2(µmol)	-1.141E+07	9.392E+06	-1.214	0.270	0.013
CO_3(µmol)	-8.227E+06	1.215E+07	-0.677	0.524	0.281
HCO_3(µmol)	-7.560E+06	1.143E+07	-0.662	0.533	0.001
DIC(µmol)	6.825E+06	1.092E+07	0.625	0.555	0.059
SST (ºC)	**-3.749**	**1.104**	**-3.396**	**0.015**	**0.373**
SSS (psu)	-3.283	2.390	-1.373	0.219	0.206
PO_4 (µmol /kg)	**-7.566**	**2.073**	**-3.650**	**0.011**	**0.333**
NO_3 (µmol /kg)	**1.410**	**0.349**	**4.039**	**0.007**	**0.206**
Si (µmol /kg)	-0.864	0.391	-2.208	0.069	0.045
O2 (mL/L)	-1.303	1.199	-1.087	0.319	0.395
ALK	0.698	1.168	0.598	0.572	0.164
pCO_2 ~1850	**0.444**	**0.077**	**5.777**	**0.001**	**0.438**

Table 2b: As Table 2a, but with $\varepsilon_{p\text{-}DIC}$ as dependent variable.

	Coeff.	Std.err.	t	p	R^2
Constant	132.4	59.4	2.227	0.068	
CO_2(µmol)	-1.137E+07	9.267E+06	-1.227	0.266	0.004
CO_3(µmol)	-8.365E+06	1.199E+07	-0.698	0.512	0.052
HCO_3(µmol)	-7.665E+06	1.127E+07	-0.680	0.522	0.021
DIC(µmol)	6.899E+06	1.077E+07	0.641	0.545	0.057
SST (ºC)	**-3.890**	**1.089**	**-3.571**	**0.012**	**0.055**
SSS (psu)	-3.371	2.358	-1.430	0.203	0.117
PO_4 (µmol /kg)	**-7.627**	**2.045**	**-3.729**	**0.010**	**0.100**
NO_3 (µmol /kg)	**1.416**	**0.344**	**4.112**	**0.006**	**0.011**
Si (µmol /kg)	-0.873	0.386	-2.260	0.065	0.001
O2 (mL/L)	-1.299	1.183	-1.098	0.314	0.070
ALK	0.728	1.152	0.632	0.551	0.071
pCO_2 ~1850	**0.446**	**0.076**	**5.881**	**0.001**	**0.113**

600